Automated Diagnosis of Covid-19 and Pneumonia Using Transfer Learning and Custom Segmentation on Chest X-Ray Images

ADVAIT K ASOK, LIDIYA LILLY THAMPI
Department of Computer Science & Engineering,
Indian Institute of Information Technology, Kottayam (IIITK),
Valavoor P.O, Pala Kottayam,
INDIA

Abstract: - The key goals of this study are to discover, demonstrate, and quantify advancements in deep learning approaches for classifying healthy, pneumonia of the community-acquired and viral types, and COVID-infected lungs from X-ray images and to learn how the pre-trained models react to the training with custom segmented images. The proposed model uses the dataset pre-processed to generate unique masks and segment the lung region to train a convolutional neural network with a transfer learning model using VGG16 and VGG19 architecture. The accuracy and F1 score results for 3-way classification with custom processing are high for VGG19 with custom segmentation. In contrast, the results for the 4-way classification were stable with and without custom processing for both VGG16 and VGG19 models.

Key-Words: - Lung Segmentation, Transfer Learning, Chest X-Ray Image, Pneumonia, COVID-19, Image Processing.

Received: April 23, 2023. Revised: April 9, 2024. Accepted: May 11, 2024. Published: June 25, 2024.

1 Introduction

Getting a chest x-ray (CXR) has always been the best way to tell if someone has pneumonia or a COVID-19 infection. Radiography's benefits include its familiarity with patients, low cost compared to newer modalities like CT, seamless incorporation into electronic medical records, and widespread acceptance among medical professionals. Low sensitivity in detecting a variety of diseases, such as pulmonary edema and pneumothorax, are two of its major downsides, [1]. Bacterial pneumonia is caused by streptococcus pneumoniae, while viral pneumonia is caused by viruses, characterized by fever, cough, muscle aches, and sore throat, [2].

CXR image requires a professional and takes up a lot of time for analysis as the X-rays of bacterially acquired pneumonia typically show a white concentrated patch of porosity, while viral acquired pneumonia typically shows widespread lung involvement, [3]. This can lead to misdiagnosis, delay in treatmen t, and increased cost of treatment [4]. RT-PCR method is used to diagnose COVID-19 but requires expensive equipment and at least 24 hours for a viable result, [5]. Several studies have combined three-way categorization of X-ray images along with four-way categorization to distinguish between COVID-19, viral and bacterial pneumonia, and healthy lungs [6]. In this paper, CXR pictures are used for transfer learning using VGG16 and VGG19, as well as several image processing techniques including adaptive histogram equalization, grey scaling, binary threshold, black-hat morphology, feature extraction, and contouring to categorize and improve diagnostic accuracy by forming a custom processed dataset by separating cases of COVID infected lung, viral and bacterial pneumonia infected lung, and a healthy lung. The VGG19 method highly improved the model's precision, reliability, and F1 score compared to previous segmentation and categorization methods.

2 Related Work

Using CXR images to diagnose lung diseases like COVID-19 and pneumonia, machine-learning algorithms have recently acquired traction in the medical world.

In an analysis with 40 analogue chest CXRs from patients with normal and pneumonia situations, [7], images were cropped and the lung region was extracted using methods developed in-house. To differentiate between normal lung tissue and diseased haze, Otsu thresholding was used to detect pneumonia clouds. Healthy lung area as a percentage of total lung area has been proposed to be calculated to conclude.

By analyzing chest X-rays, suggested a deep-learning CNN model be used to differentiate between cases of healthy people, COVID-19, and viral pneumonia in the lungs, [8]. The proposed model uses VGG16-based pre-trained ImageNet weights. The model was improved by adding new, custom-made layers. VGG16 has an accuracy score of 92.7%. A system was developed for transfer learning and tested several deep-learning models using data from COVID-19, viral pneumonia, and pictures of normal lung CXR with counts at 423, 1485, and 1579, [9]. To classify the two methodologies, the networks were trained using healthy and COVID-induced pneumonia-infected lung CXR pictures as well as normal, viral, and COVID-induced pneumonia-infected X-ray images with and without image augmentation. Both systems were 99.7 and 97.1 percent accurate in their classifications, respectively, while their specificity was 99.55 and 98.1 percent, respectively. However, it did not meet the criteria for bacterial pneumonia.

In a recent study, multiple Convolutional Neural Networks were trained to classify x-ray images as either pneumonia or non-pneumonia by altering the network's parameters, hyper-parameters, and number of convolutional layers, [10]. Six distinct models are covered in the research. One similarity between the two models is the presence of two convolutional layers. There are also four alternative trained models available, including VGG16, VGG19, ResNet50, and Inception-v3. The validation accuracy for the first model is 85.26%, while the second model is 92.31%. 87.28 percent is the accuracy of VGG16, 88.46 percent of VGG19, 77.56 percent of ResNet50, and 70.99 percent of Inception-v3.

To the best of my knowledge, this study is the first to examine how segmented lung areas from X-ray images might be used as input for classification algorithms to perform better

3 Materials and Methods

DL methods require data retrieval, processing, training, analyzing, optimizing, and classifying. After the models have been trained on the novel auto-segmented dataset, we'll test how well the models trained with and without custom segmentation methods can distinguish between healthy, COVID-19, bacterial, and pneumonia caused by viruses in CXR pictures. Figure 2 represents the methods we follow in this study.

3.1 Chest X-Ray Image Dataset

Images of the chest X-rays were taken from the Mendeley data repository. Figure 1 depicts the current data set of 9208 images which includes 1,281 images of COVID-19 infected, 3270 images of healthy, 1656 images of viral pneumonia-infected, and 3001 images of bacterial pneumonia infected lung CXR, [11]. For the study, we will consider a total of 5000 images, with 1250 images chosen at random from each group.

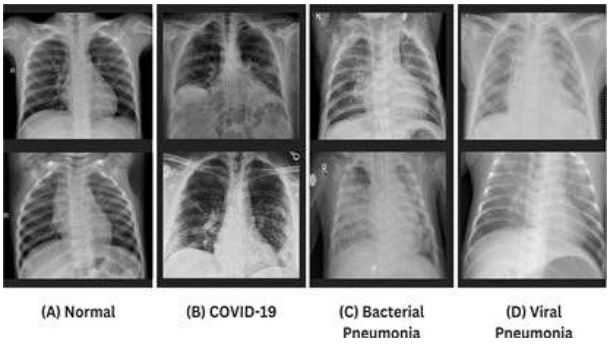

Fig. 1: Images of posterior-anterior chest X-rays from COVID-19: A Curated Dataset (X-Rays), [11]

3.2 Custom Lung Segmentation

The original images were of high resolution and varied sizes. As per the observations from Table 1, to make the computation and training faster and to generate a better-segmented image of CXR the images were resized to 256 x 256 pixels, [12]. To guarantee the achievement of the dynamic signal intensity, imaging data must be standardized and converted to a gray-scale range of [0, 1] or [-1, 1], [13].

Implementation of the custom segmentation workflow is explained in Figure 3 (A) vertical line with a center offset is drawn on the image at the place of the maximum pixel sum to improve the lung boundary identification, [7], as shown in Figure 3 (B). The images with the center line erased will be subjected to Contrast-Limited Adaptive Histogram Equalization to boost image quality, as depicted in Figure 3 (C), [14], [15].

The "Blackhat" morphological operation is applied to the CLAHE-processed CXR pictures to boost the image's dark regions, [16], [17], as shown in Figure 3 (D). The average pixel intensity value as the threshold is applied to the image with black-hat morphology, setting all pixels with intensities greater than the mean to 255 and all pixels with values less than the mean to 0, [18]. The result is shown in Figure 3 (E).

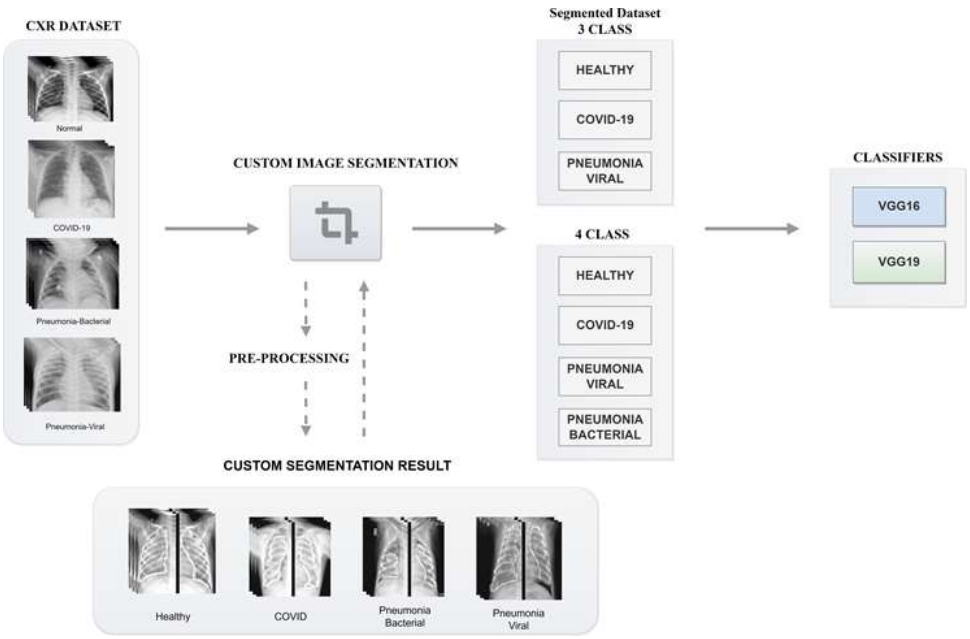

Fig. 2: Proposed architecture diagram

Table 1. The image size and custom segmentation time comparison

Data count	Image shapes	Segmentation time (s)	Output
5000	(499, 406), (645, 715), (450. 462), (300, 400), etc.	933.028	 Ambiguous
	(256, 256)	177.905	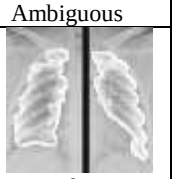 Unambiguous

The corner mask image is then returned with the detected corners highlighted in white and the rest of the image in black, as shown in Figure 3 (F). The Corner-circle mask, which is a binary mask image with circular areas around the corners, and the binary thresholded image will be multiplied element by element to make the array mask as portrayed in Figure 3 (G). The median blur is applied as shown in Figure 3 (H). The list of contours is retrieved, [19], as depicted in Figure 3 (I). This morphological dilation operation is applied, [20], as depicted in Figure 3 (J). Overlaying the mask on the CXR creates a new image, as shown in Figure 3 (K), by performing an arithmetic operation that adds two input images together using their relative weights. Created a new image in which the areas outside the mask are blackened out while the areas within the mask remain unchanged, as shown in Figure 3 (L).

3.3 CXR Classification with Transfer Learning

In this study, the custom segmented image dataset will be trained using transfer learning methodologies, and there will be two categorizations for the chest X-rays: Lung health

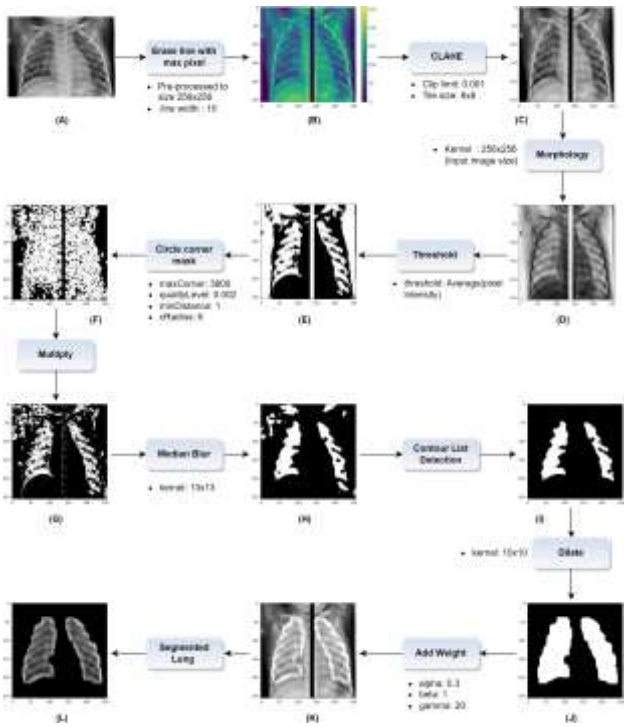

Fig. 3: Proposed custom segmentation workflow

is classified as either (i) three classes (healthy lungs, covid infected lung, and viral pneumonia) (ii) four classes (healthy lungs, covid infected lung, viral pneumonia, and bacterial pneumonia) using the pre-trained VGG16 and VGG19 models

Additionally, the efficacy of the VGG16 and VGG19 models trained without a segmented image dataset is compared.

4 Results and Outcomes

4.1 Experimental Design

The experiment was built using the Google Colab platform and a Python 3 (GPU) backend for Google Compute Engine. Multiplying arrays of input data and output weights by a matrix during CNN training is a computationally intensive process, [8]. The use of Kaggle notebooks facilitated rapid training, computing, and data administration.

4.1.1 Dataset Splitting

As shown in Figure 4, a random reordering is performed on all the picture filenames in the root Curated dataset directory with a total of 5000 images with 1250 images in each class and sorted into three distinct piles based on the specified train ratio (60%), validate ratio (10%), and test ratio (30%).

4.1.2 Performance Measurement

The starting settings for the learning rate, epochs, and number of batches are 0.0001 or 20 and 32 or 128, respectively, [21].

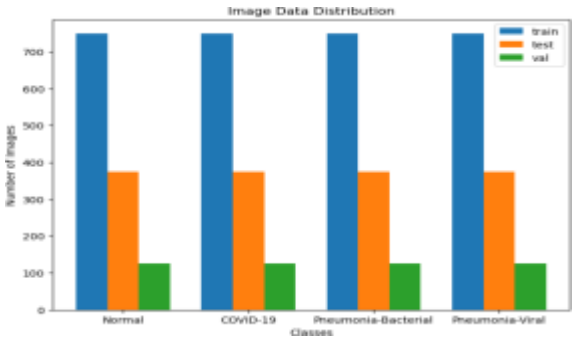

Fig. 4: CXR image distribution on test, train, and validation

The efficacy of the trained models is evaluated using accuracy and sensitivity. The confusion matrix is used to compare the proportions of true positives, true negatives, false negatives, and false positive detections to assess the accuracy of a model.

4.2 Evaluation of Three-Class Classification with Custom Segmented Data

Using the custom segmented image dataset generated in the earlier stage of this study, we are currently performing the initial stage of training a VGG16 and VGG19 model to distinguish between COVID-19, viral pneumonia, and a healthy lung. The results are compared between training on non-segmented plain X-ray pictures and training on CXR images that have been pre-processed utilizing the unique segmentation method developed for this research, [22].

4.2.1 Transfer Learning with VGG16

For 100 epochs, it is observed that the model was able to accurately categorize 97.33% of the data points at an early stopping of 30 epochs as shown in Figure 5 (A). With a precision of 0.9734, the model correctly predicted 97.34% of the cases it labeled as positive. The model has a recall of 0.9733, therefore it was able to properly identify 97.33% of all true positives. The model successfully found 98.66% of false negatives and 1.33 percent of negatives as positives. The model acquired 0.9733 as the F1-score representing a fair harmony between the precision and the recall.

4.2.2 Transfer Learning with VGG19

According to the classification discussed in Figure 5 (C), the F1 score of 0.9742 was reached by the model VGG19 in terms of accuracy, recall, and precision. A score of 0.0138 is received as the false positive rate and a specificity score is 0.9862. Top scores for these tests suggest that the VGG 19 model is effective in categorizing COVID-19, two types of pneumonia, and normal healthy lung images from a chest X-ray trained on the custom segmentation methods. It can be assumed that with more training on larger, clearer CXR images and a more varied dataset, the model's efficiency and universality could be improved.

4.3 Evaluation of Four-Class Classification with Custom Segmented Data

Performed the second stage of training a VGG16 and VGG19 model to distinguish between COVID-19, bacteria-induced pneumonia, viral pneumonia, and a healthy lung.

4.3.1 Transfer Learning with VGG16

For 100 epochs, VGG16 has a false positive rate of 0.052 and an F1- score of 0.8441, accurately predicting 84.46% at an early stopping of 17.5 epochs as seen in Figure 5 (B). A precision of 0.8435, recall of 0.8446, and specificity of 0.9482 suggest that the model is missing some true positives. The custom segmented data training did not result in a high improvement in the

performance of VGG-16 classifying the images into the 4 categories.

4.3.2 Transfer Learning with VGG19

As per the classification for 100 epochs, an accuracy of 0.844 suggests that almost 84 percent of the dataset was properly identified by the VGG19 model in 20 epochs as depicted in Figure 5 (D). The model's precision is 84.16%, which means that more than three-quarters of the positive samples were indeed positive. This statistic helps gauge how well the model suppresses spurious positive results. Out of all the true positive samples in the dataset, the model accurately identified almost 84 percent of them. Since 94.8 percent of the true negative samples in the training set were accurately identified as such, the model has a specificity of 0.948. Approximately 5.2 percent of the true negative samples in the training set were mistakenly labeled as positive.

The model's F1-Score, a measure of its overall performance in terms of accuracy and recall equal to the harmonic mean of these two metrics, is 0.8428. Based on these measures, it appears that the VGG19 model did a decent job of categorizing the samples, but it might use some more work, especially in the areas of false positives and false negatives.

4.4 Performance Comparison with Non-Segmented Images

4.4.1 Transfer Learning with VGG16

For a 3-class classification, it is observed that with an accuracy of 97.51%, the model was successful in classifying all the cases. The model's precision was 0.9751, which suggests that 94.97% of positive cases were indeed positive. With a specificity of 0.9875, the model successfully identified the false negatives, and 1.2% of negative cases were incorrectly classified as positives.

The model had an F1-score of 0.9751, which is the harmonic mean of precision and recall and represents how well they are balanced. Collectively, these findings are indicative of the model's low false positive rate and high accuracy and precision in instance classification. According to the F1-score, the model also struck a reasonable balance between precision and recall, and the curves are shown in Figure 6 (A).

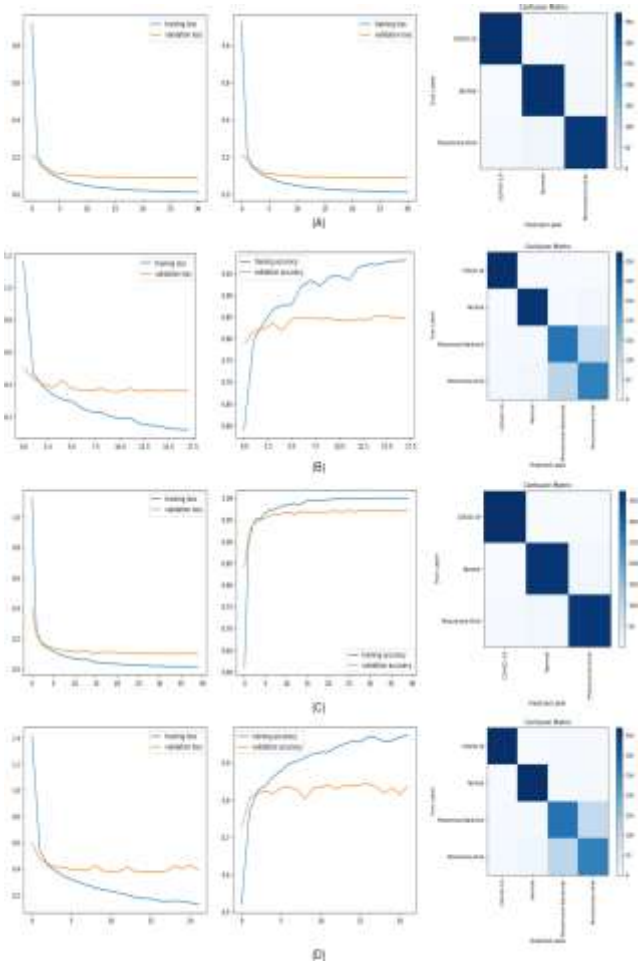

Fig. 5: Segmented Dataset Classification
A) VGG-16 3 class B) VGG-16 4 class
C) VGG-19 3 class D) VGG-19 4 class

For the 4-way classification, the model has an F1-score of 0.8556 and an accuracy of 85.53 % after an early stop at 20 epochs as shown in Figure 6 (B). From the metrics depicted in Table 2, we can infer that a respectable fraction of true positives is being identified by the model and that it can accurately identify a sizable fraction of the data.

Table 2. VGG-16 performance metrics

Classifier	VGG-16			
Parameters	3 Class		4 Class	
	non-segmented	segmented	non-segmented	segmented
Accuracy	97.51	97.33	85.53	84.46
Precision	97.51	97.34	85.59	84.35
Recall	97.51	97.33	85.53	84.46
Specificity	98.75	98.66	95.17	94.82
False Positive	0.0133	0.025	0.0482	0.0517
F1-Score	0.9751	0.973	0.8556	0.8441

A very small proportion of samples may have been misclassified by the model as diseased due to the false positive rate of 0.025 in the 3-way

classification than the 4-way classification with segmented data with the score of 0.0517.

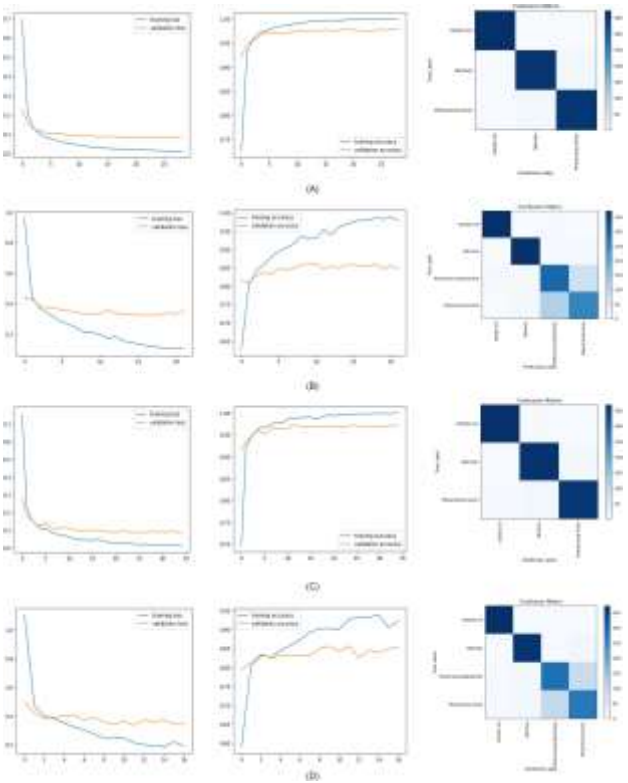

Fig. 6: Non-segmented dataset classification
A) VGG-16 3 class B) VGG-16 4 class
C) VGG-19 3 class D) VGG-19 4 class

The model works efficiently with the 3-class categorization meanwhile the 4-class categorization accuracy slightly decreases when the dataset is processed through custom processing, resulting in lower categorization precision.

4.4.2 Transfer Learning with VGG19

The model successfully labeled 96.97% of the test dataset at an early stopping of 35 epochs as depicted in Figure 5 (C). The F1-score of 0.9698 and the other metrics shown in Table 3 further indicate that the model struck an adequate balance between accuracy and recall. All things considered, VGG19 appears to be a very efficient model for dividing chest X-rays into three distinct groups when the custom segmentation process is applied to the dataset.

For a 4-way classification with an accuracy of 85.67% and F1 score of 0.855, the VGG19 model proved capable of correctly categorizing the test data. The model was accurate 85.51% of the time when predicting a class label (precision= 0.8551). From the metrics shown in Table 3 and Figure 5 (D), it seems that 4.78 percent of erroneous negatives were mislabeled as true positives. When we compare the algorithms for the two types of classification, we can conclude that 3-class categorization improves when custom segmentation is applied to the dataset, whereas 4-class categorization accuracy slightly decreases when the dataset is processed through custom processing, resulting in lower categorization precision.

Table 3. VGG-19 performance metrics

Classifier	VGG-19			
Parameters	3 Class		4 Class	
	Non-seg	Seg.	Non-seg.	Seg.
Accuracy	96.9	97.2	85.6	84.40
Precision	96.9	97.2	85.5	84.16
Recall	96.9	97.2	85.7	84.40
Specificity	98.5	98.6	95.2	94.80
FPR	0.02	0.01	0.05	0.052
F1-Score	0.96	0.97	0.85	0.842

5 Discussion

High levels of accuracy, precision, recall, and F1-score were achieved in VGG16 than VGG19 when used to categorize X-rays into three groups: viral pneumonia, COVID-19 infected, and healthy lungs. More specifically, VGG19 outperformed a bit more than VGG16 in the categorization of X-rays into three groups job, suggesting it is more suited to it. However, there is room for improvement in the custom segmentation approach used in this research. Particularly bacterial pneumonia and some chest X-rays with comparatively large clouded lung regions tend to produce less accurate segmentation. We need more research to see how other state-of-the-art models, like EfficientNet, [23], stack up against VGG19. The impressive architecture and computational elements, the EfficientNet results in impressive accuracy in the image categorization tasks. It would be an interesting experiment to compare the metrics generated with EfficientNet, VGG19, and VGG16.

6 Conclusion

The classification with VGG19 resulted in a higher accuracy score for the 3-way categorization of the X-ray images. It suggests that the custom segmentation discussed in this paper enhances the performance of the model.

The 3-way categorization without the custom segmentation resulted in the F1 score of 97.51 percent and 0.9751 respectively for VGG16 and 96.97 percent and 0.9698 for VGG19. The results for the 4-way classification were 85.53 percent and

0.8556 for VGG16 and 85.66 percent and 0.8558 for VGG19. Scores of 97.33 percent, 0.9733 for VGG16 and 97.24 percent, 0.9724 for VGG19 in 3-way classification, and 84.46 percent, 0.8441 for VGG16 and 84.40 percent, 0.8428 for VGG19 in 4-way classification were observed using custom segmentation.

Future studies may refine the custom segmentation approach and apply it to the dataset without ground truth to better isolate lung areas and minimize image noise, improving multi-classification of lung X-rays. We may use Jaccard similarity coefficients and Dice coefficients to compare manual and automated segmentation.

The results of the study show that multi-class categorization of chest X-rays, which can assist in the early identification and treatment of respiratory disorders, can be much improved by employing transfer learning techniques in conjunction with bespoke lung segmentation.

References:

[1] Hunton, Ryan. "Updated concepts in the diagnosis and management of community-acquired pneumonia." JAAPA: *Official Journal of the American Academy of Physician Assistants*, vol. 32, no. 10, pp. 18-23, 2019, doi: 10.1097/01.JAA.0000580528.33851.0c.

[2] S. Serte and A. Serener, "Discerning COVID-19 from mycoplasma and viral pneumonia on CT images via deep learning," *2020 4th International Symposium on Multidisciplinary Studies and Innovative Technologies (ISMSIT)*, Istanbul, Turkey, pp. 1-5, 2020, doi: 10.1109/ISMSIT50672.2020.9254970.

[3] Popovsky, Erica Y., and Todd A. Florin. "Community-Acquired Pneumonia in Childhood." *Encyclopedia of Respiratory Medicine*, pp. 119–131, 2022, doi: 10.1016/B978-0-08-102723-3.00013-5.

[4] Abdullahi Umar Ibrahim, Mehmet Ozsoz, Sertan Serte, Fadi M. Al-turjman, and Polycarp Shizawaliyi Yakoi. "Pneumonia Classification Using Deep Learning from Chest X-ray Images During COVID-19." *Cognitive computation*, pp. 1-13, 4 Jan. 2021, doi: 10.1007/s12559-020-09787-5.

[5] Islam, N., Salameh, J., Leeflang, M.M., Hooft, L., McGrath, T.A., van der Pol, C.B., Frank, R.A., Kazi, S., Prager, R., Hare, S.S., Dennie, C., Spijker, R., Deeks, J.J., Dinnes, J., Jenniskens, K., Korevaar, D.A., Cohen, J.F., Van den Bruel, A., Takwoingi, Y., van de Wijgert, J.H., Wang, J., & McInnes, M.D. "Thoracic imaging tests for the diagnosis of COVID-19." *The Cochrane database of systematic reviews*, vol. 3, no. 3, p. CD013639. 16 Mar. 2021, doi: 10.1002/14651858.CD013639.pub4

[6] Tiwari, Alok, Taresh Sarvesh Sharan, Shiru Sharma, and Neeraj Sharma. "Deep learning-based automated multiclass classification of chest x-rays into covid-19, normal, bacterial pneumonia and viral pneumonia". *Cogent Engineering*, vol. 9, no. 1, 2022, https://doi.org/10.1080/23311916.2022.2105559.

[7] A. Sharma, D. Raju and S. Ranjan, "Detection of pneumonia clouds in chest X-ray using image processing approach," *2017 Nirma University International Conference on Engineering (NUiCONE)*, Ahmedabad, India, pp. 1-4, 2017, doi: 10.1109/NUICONE.2017.8325607.

[8] Verma, Dhirendra Kumar, Gaurav Saxena, Amit Paraye, Alpana Rajan, Anil Rawat, and Rajesh Kumar Verma. "Classifying COVID-19 and Viral Pneumonia Lung Infections through Deep Convolutional Neural Network Model using Chest X-Ray Images." *Journal of medical physics*, vol. 47, no. 1, pp. 57-64, 2022, doi: 10.4103/jmp.jmp_100_21.

[9] Chowdhury, M.E., Rahman, T., Khandakar, A., Mazhar, R., Kadir, M.A., Mahbub, Z.B., Islam, K.R., Khan, M.S., Iqbal, A., Al Emadi, N. and Reaz, M.B.I. "Can AI Help in Screening Viral and COVID-19 Pneumonia?," in *IEEE Access*, vol. 8, pp. 132665-132676, 2020, doi: 10.1109/ACCESS.2020.3010287.

[10] Rachna Jain, Preeti Nagrath, Gaurav Kataria, V. Sirish Kaushik, D. Jude Hemanth, "Pneumonia detection in chest X-ray images using convolutional neural networks and transfer learning". *Measurement*, Vol. 165, p. 108046, 2020, doi: 10.1016/j.measurement.2020.108046.

[11] Sait, Unais; Lal KV, Gokul; Prakash Prajapati, Sunny; Bhaumik, Rahul; Kumar, Tarun; Shivakumar, Sanjana; Bhalla , Kriti, "Curated Dataset for COVID-19 Posterior-Anterior Chest Radiography Images (X-Rays).", Mendeley Data, V3, 2020, doi: 10.17632/9xkhgts2s6.1.

[12] H. T. Thanh, P. H. Yen and T. B. Ngoc, "Pneumonia Classification in X-ray Images Using Artificial Intelligence Technology," *2020 Applying New Technology in Green Buildings (ATiGB)*, Da Nang,

Vietnam, pp. 25-30, 2021, doi: 10.1109/ATiGB50996.2021.9423017.

[13] S. Walvekar and S. Shinde, "Efficient Medical Image Segmentation Of COVID-19 Chest CT Images Based on Deep Learning Techniques," *2021 International Conference on Emerging Smart Computing and Informatics (ESCI)*, Pune, India, 2021, pp. 203-206, doi: 10.1109/ESCI50559.2021.9397043.

[14] R. I. Bendjillali, M. Beladgham, K. Merit, A. Taleb-Ahmed, "Illumination-robust face recognition based on deep convolutional neural networks architectures," *Indonesian Journal of Electrical Engineering and Computer Science*, vol. 18, no. 2, May 2020, pp. 1015–1027, doi: 10.11591/ijeecs.v18.i2.pp1015-1027.

[15] B. K. Umri, M. Wafa Akhyari and K. Kusrini, "Detection of Covid-19 in Chest X-ray Image using CLAHE and Convolutional Neural Network," *2020 2nd International Conference on Cybernetics and Intelligent System (ICORIS)*, Manado, Indonesia, pp. 1-5, 2020, PMID: 11701515, doi: 10.1109/ICORIS50180.2020.9320806.

[16] A. Mordvintsev, K. Abid, "Opencv-python tutorials documentation," 2017, [Online]. https://opencv24-python-tutorials.readthedocs.io/_/downloads/en/stable/pdf/ (Accessed date: April 12, 2022).

[17] Konkol, Marek & Śniatała, Konrad & Śniatała, Paweł & Wilk, Szymon & Baczyńska, Beata & Milecki, Piotr, "Computer Tools to Analyze Lung CT Changes after Radiotherapy". *Applied Sciences*, vol. 11, no. 04, MDPI, p. 1582, 2021, doi: 10.3390/app11041582.

[18] Pham, Dzung L., Chenyang Xu, and Jerry L. Prince. "Current methods in medical image segmentation." *Annual Review of Biomedical Engineering*, vol. 2, no. 1, pp. 315-337, 2000, doi: 10.1146/annurev.bioeng.2.1.315.

[19] M. M. Hasan, M. Md. Jahangir Kabir, M. R. Haque and M. Ahmed, "A Combined Approach Using Image Processing and Deep Learning to Detect Pneumonia from Chest X-Ray Image," *2019 3rd International Conference on Electrical, Computer & Telecommunication Engineering (ICECTE)*, Rajshahi, Bangladesh, December 26, 2019, pp. 89-92, doi: 10.1109/ICECTE48615.2019.9303543.

[20] M. N. Saad, Z. Muda, N. S. Ashaari and H. A. Hamid, "Image segmentation for lung region in chest X-ray images using edge detection and morphology," *2014 IEEE International Conference on Control System, Computing and Engineering (ICCSCE 2014)*, Penang, Malaysia, 2014, pp. 46-51, doi: 10.1109/ICCSCE.2014.7072687.

[21] Pramanik, R., Sarkar, S. and Sarkar, R., "An adaptive and altruistic PSO-based deep feature selection method for Pneumonia detection from Chest X-rays." *Applied Soft Computing*, vol. 128, 2022, p. 109464, doi: 10.1016/j.asoc.2022.109464

[22] Wang, L., Zhang, Y., Wang, D., Tong, X., Liu, T., Zhang, S., Huang, J., Zhang, L., Chen, L., Fan, H. and Clarke, M., "Artificial Intelligence for COVID-19: A Systematic Review." *Frontiers in medicine*, vol. 8, p. 704256. 30 Sep. 2021, PMID: 34660623, PMCID: PMC8514781, doi: 10.3389/fmed.2021.704256.

[23] Talukder, M.A., Layek, M.A., Kazi, M., Uddin, M.A. and Aryal, S., "Empowering COVID-19 detection: Optimizing performance through fine-tuned EfficientNet deep learning architecture." *Computers in Biology and Medicine*, vol. 168, 2024, p. 107789, doi: 10.1016/j.compbiomed.2023.107789.

Contribution of Individual Authors to the Creation of a Scientific Article (Ghostwriting Policy)

The authors equally contributed to the present research, at all stages from the formulation of the problem to the final findings and solution.

Sources of Funding for Research Presented in a Scientific Article or Scientific Article Itself

No funding was received for conducting this study.

Conflict of Interest

The authors have no conflicts of interest to declare.